Ocean and Coastal Research

CASE REPORT

http://doi.org/10.1590/2675-2824072.23200
ISSN 2675-2824

Insights into the flow characteristics of tsunami bores and surges: a case study of Malaysian coastline

Wei Chek Moon*[1,2], Tze Liang Lau[2], How Tion Puay[3]

[1] Faculty of Engineering – Technology & Built Environment – UCSI University (56000 Cheras – Kuala Lumpur – Malaysia).
[2] School of Civil Engineering – Universiti Sains Malaysia (14300 – Nibong Tebal – Pulau Pinang – Malaysia).
[3] River Engineering and Urban Drainage Research Centre – Universiti Sains Malaysia (14300 – Nibong Tebal – Penang – Malaysia).

* Corresponding author: vmoonpower@yahoo.com.my

ABSTRACT

Tsunamis, despite their rarity, are among the deadliest natural disasters, inflicting catastrophic damage on both coastal and inland regions. Given their highly site-specific impact, a comprehensive understanding of tsunami wave flow characteristics is crucial for effective tsunami preparedness and for safeguarding civil engineering structures. This study investigates the formation and progression of tsunami bores as they transition into surges near the shore. We employed a wave-flume experimental approach, with a specific focus on the Malaysian coastline. Experiments took place in a wave flume with a length of 40 m and a platform designed to replicate the gentle slopes commonly found in Malaysian coastal areas vulnerable to tsunamis. The primary focus lied in measuring key flow parameters, including flow depths and velocities near the shore. Wet bed bores were marked by a sudden rise in water depth and considerable air entrainment in the front region. As these waves transformed into dry bed surges, the front slope became gentler, and aeration diminished, while peak velocities increased. Additionally, the study also delves into the relations between flow depth and velocity concerning Froude numbers and momentum flux. The outcomes contribute significantly to global initiatives aimed at improving coastal resilience against tsunamis.

Keywords: Tsunami-like waves, Malaysian shore profile, Flow depths, Velocities, Momentum flux

INTRODUCTION

Catastrophes like tsunamis involve unsteady flow motions that result in a rapid rise in water level, associated with human casualties and significant infrastructure damage. The world witnessed the destructive force of tsunamis in 2004 when a massive magnitude 9.3 earthquake triggered the Indian Ocean Tsunami (IOT) in Banda Aceh. This catastrophic event caused widespread devastation, claiming hundreds of thousands of lives and causing economic losses amounting to billions of dollars (Heger and Neumayer, 2019; Ahmadun et al., 2020; Oktari et al., 2021; Moon et al., 2022). While understanding the physical phenomenon is crucial for better coastal protection, the complex nature of tsunami waves, coupled with variations in flow depth and velocity over time, presents challenges in addressing these intricate tasks.

As the tsunami advances toward shallow coastal areas, it experiences a swift change

Submitted: 17-Dec-2023
Approved: 18-Jun-2024

Associate Editor: Piero Mazzini

characterized by a reduction in speed and a rise in wave height due to energy dissipation, while maintaining a constant total energy flux (Nelson, 2011). This phenomenon, known as the "shoaling" effect, follows the conservation of energy theory, where kinetic energy undergoes conversion into potential energy as the tsunami decelerates. This results in a significant rise in wave height as the tsunami approaches coastal zones. Upon nearing the shore, especially in areas with reduced water depth in the runup zone, the wave height further increases, and the wave-breaking processes occurs, sometimes transforming into a step-like wave with steep breaking (Yeh and Mok, 1990). The term "bore" describes the turbulent and aerated appearance of a broken wave, also referred to as a "surge" as it travels across the land.

Heller et al. (2005) explored the essential hydraulic aspects of tsunami runup, categorizing the wave-breaking process into several stages such as wave-shoaling, front overturns, bore development, and substantial air entrainment into the wave front. Chanson (2006) later drew similarities in the instantaneous free surface flow profiles between tsunami-induced bores and dam-break flow. In 2012, Klettner et al. (2012) contributed with additional insights into wave breaking and bore formation onshore. They observed depression waves in laboratory experiments and confirmed the development of shoreline recession, followed by a hydraulic bore that runs up on the beach during a tsunami.

Back in 1988, Yeh and his co-researcher conducted extensive research to study the bore transition phase to wave runup on a uniformly sloping beach. From Yeh and Ghazali (1988), the observed transition process was notably different from the nature of complete bore collapse, leading to deduce that momentum exchange occurred between the bore and water body along the shore. In the experiments, the bore front did not directly approach the shoreline; instead, it pushed forward a quiescent mass of water, initiating the runup motion of a small wedge-shaped water body along the shore. In the case of weak or undular bores, the bore front, consisting of a turbulent crest, directly overturned onto the beach, resembling the overturning front of wave breaking on a steep slope. The hydrodynamic features of waves moving across dry and wet bed conditions were also experimentally demonstrated by Cross (1967), Ramsden (1996), Nouri et al. (2010), and a recent study by Wüthrich et al. (2018).

While the previous contributions offered insights into the flow mechanisms, specifically bore and surge dynamics, challenges persist in understanding tsunami bores progress and transform into surges near the shore. To address this gap, this study conducts a series of physical experiments to replicate and examine the characteristics of tsunami-like wave flow near the shore. Focusing on the Malaysian coastline as a case study, we aim to provide fresh insights into the progression of tsunami bores as they transform into surges near the shore.

STUDY AREA

In the case of no exception, Malaysia was not spared from the 2004 IOT. The northern coastal areas of West Malaysia (also referred to as Peninsular Malaysia), specifically in Kuala Muda and the surrounding islands such as Penang Island and Langkawi Island, were among the hardest-hit regions. This unprecedented tsunami event left a profound impact in the country, leading to the confirmed death of 68 individuals, extensive environmental and structural damage, and significant socio-economic consequences for the affected communities (Abdullah et al., 2005). Shaluf and Ahmadun (2006) even described it as one of the most significant disasters out of the 39 that had befallen Malaysia between 1968 and 2004.

The occurrence of a rare tsunami event in Malaysia presented a unique opportunity to validate tsunami simulation models using field data for comparison. Local researchers have increasingly focused on investigating potential worst-case tsunami scenarios (Mokhtar et al., 2008; Dao et al., 2009; Koh et al., 2009; Liu et al., 2009; Karim et al., 2010; Pedersen et al., 2010; Adam, 2011; Ismail and Wahab, 2011; Teh et al., 2011; Mazni, 2012; Basri et al., 2013; Nurashid et al., 2013). Despite the absence of subsequent

tsunami disasters since 2004, the computational simulations carried out in these studies have revealed that Malaysia's coastal areas may face a looming tsunami threat, particularly if tsunamigenic earthquakes occur in regions such as the Andaman Nicobar Islands fault slip zone, Philippine subduction zones, the South China Sea, Sulawesi Sea, and the Makassar Strait. In an effort to raise public awareness about potential tsunami occurrences, the Ministry of Science, Technology and Innovation of Malaysia (MOSTI) has developed a tsunami hazard map (Figure 1(a)) for Malaysia, highlighting the northwestern part of Peninsular Malaysia and the northeast, northwest, and southwest coasts of Sabah as highly vulnerable hazard zones (MOSTI, 2009).

In determining the shore profile along Malaysia's highly vulnerable tsunami hazard zones, an evaluation was conducted using 30 arc-seconds bathymetry data covering the Greater Indian Ocean. This data was sourced from the Gridded Bathymetric Data Sets provided by the General Bathymetric Chart of the Oceans (GEBCO). The bathymetry data was converted into ASCII text format, indicating coordinates and heights, with the aid of the GEBCO Digital Atlas Software Interface. Subsequently, the exported grid data underwent processing by Surfer 11, to generate bathymetric contours and coastlines. Following the acquisition of the bathymetry contour, cross-sections were extracted perpendicular to the four target areas (Kuala Muda, western and northern coasts of Langkawi Island and Penang Island, as well as Sabah), representing highly vulnerable tsunami hazard zones, (Figure 1(b)) and streamlined into plane slopes (not shown herein).

Figure 1(c) depicts the typical shore profile for each target area, determined based on the previously obtained plane slopes (four profiles for Kuala Muda, five profiles for Langkawi Island, eight profiles for Penang Island, and six profiles for Sabah). It is noteworthy that, apart from Penang Island and Sabah, which also have steep slopes, all four target areas exhibit gentle slopes. These gentle slopes align with the continuous inclinations of 1:200 and 1:125, represented by a dotted line in Figure 1(c). These continuous slopes were then implemented in the study to mimic the gradual slope of typical tsunami-prone coastal regions in Malaysia.

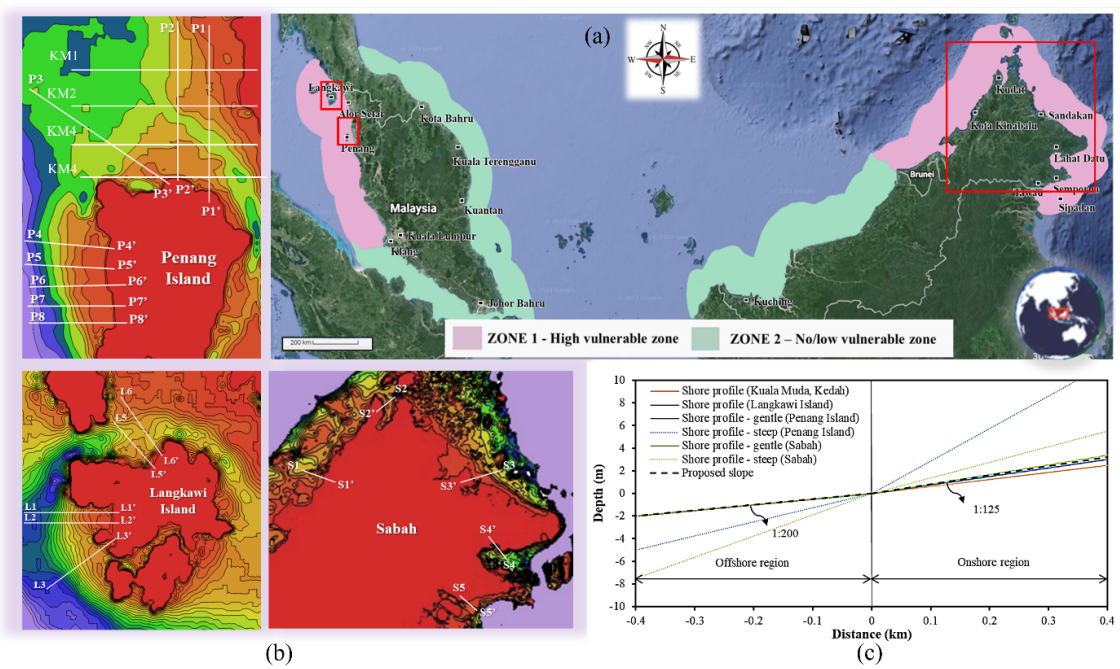

Figure 1. (a) Tsunami hazard map for Malaysia (MOSTI, 2009); (b) Bathymetry contour and (c) slope profile at Malaysian shoreline.

EXPERIMENTAL SETUP

Wave Flume Experiment

To simulate the tsunami wave dynamics along the Malaysian coastline, experiments were conducted using a 1:50 scaled wave flume at the Tsunami Laboratory in Engineering Campus of Universiti Sains Malaysia. As depicted in Figure 2, the experimental setup featured a wave flume measuring 40 m in length, 1 m in width, and 1 m in depth, constructed using gray polyvinyl chloride sheets and supported by structural steel frames at the base. This wave flume design encompassed various regions, starting with an offshore section filled with water to a depth of 470 mm. It then smoothly transitioned to the derived slope profiles, featuring continuous slopes with gradients of 1:200 and 1:125, which extended downstream from the platform and gradually shifted to the onshore region.

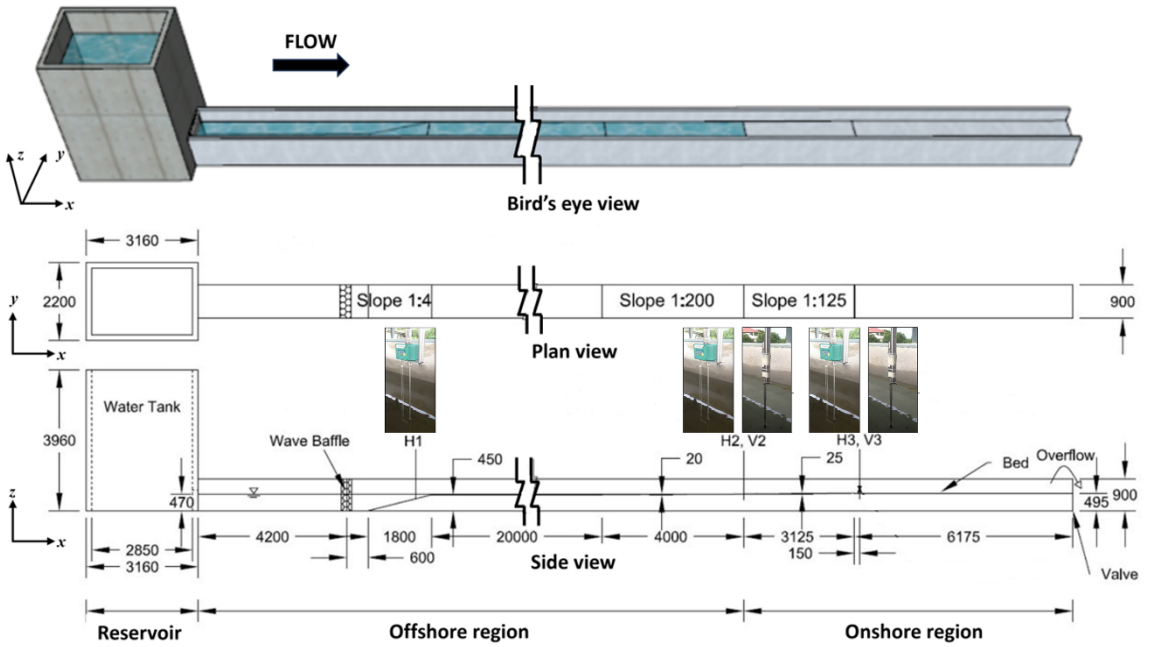

Figure 2. Schematic of experimental setup (dimension in mm).

A water tank, measuring 3 m by 2 m and standing at a height of 4 m, was connected to the wave flume. Tsunami-like waves were initiated upon releasing water impounded behind a gate and subsequently regulated by a wave baffle assembled from interlocking plastic structural modules. As these waves approached the 1:4 sloping bed, their velocity decreased, causing the wave front to progressively become nearly vertical. Eventually, the wave front transformed into a plunging type breaker and evolved into a bore. This bore then traversed the offshore region and surged up the onshore region before ending in a sump located downstream of the flume. It is essential to highlight that this study did not consider tsunami drawdown and sediment transport. Additional details about the laboratory setup are also available in Moon et al. (2020).

Instrumentation and Acquisition System

This study primary objective is to examine the flow characteristics of experimentally generated tsunami-like waves, specifically focusing on flow depths and velocities. To monitor the propagation of the wave profile, three capacitance-type wave gauges were strategically placed at different locations within the flume. These gauges were positioned at the center of the flume, with one near the offshore region (H1) and two near the shore: one at the shoreline (H2) and the other

on the horizontal dry bed section (H3), situated 3.225 m horizontally and 20 mm vertically from the shoreline, as illustrated in Figure 2. For the recording of nearshore flow velocities (V2 and V3), electromagnetic-type current meters were employed, operating at a logging frequency of 40 Hz. Specifically, V2 and V3 were respectively situated at the shoreline and on the horizontal dry bed section. To capture the waves spatial development, several camcorders operating at a frame rate of 50 frames per second were synchronized with the instrumentation.

Experimental Modeling

Three wave conditions, represented by the maximum flow depth at the horizontal dry bed section (h_{max}), were examined. As outlined in Table 1, these waves were generated by adjusting the impoundment reservoir volume within the range of 2.87 m³ to 5.52 m³. Using a Froude scaling ratio of 1:50, the 40, 70, and 100 mm wave conditions corresponded to actual wave heights of 2, 3.5, and 5 m, which allowed for recreating the documented inundation depths caused by the 2004 IOT and possible future worst scenarios along Peninsular Malaysia (discussed in Section 4.5: Flow Depth-Velocity Relationship). The wave front celerity, denoted as U, for each case was taken as the mean value from five repetitions: 1.5 m/s (h_{max} = 40 mm), 2.1 m s^{-1} (h_{max} = 70 mm), and 2.7 m s^{-1} (h_{max} = 100 mm). More details on the flow characteristics are presented and discussed in Section 4: Results.

Table 1. Summary of experimental cases.

Impoundment reservoir volume (m³)	Maximum flow depth, h_{max} (mm)	Wave front celerity, U (m s^{-1})	Surge front slope (°)
2.87	40	1.5	2.13
3.95	70	2.1	2.80
5.52	100	2.7	3.15

RESULTS

Experimental Repeatability

Each experimental case involved five test repetitions to ensure the consistency and reliability of the results, resulting in a total of 15 tests. To assess the repeatability of the experiment of generated tsunami-like waves, the measured wave profile propagation at H1 was initially examined for all three wave conditions, as depicted in Figure 3. The analysis indicates that the variation in water surface profiles among the five repetitions consistently remains below 5%. In addition to visual observations, the comparative measurements of the coefficient of determination (R^2) were employed to quantify discrepancies between the five repetitions and the mean. Figure 3 shows R^2 values of up to 0.9999, further affirming the reliability and accuracy of our dam-break wave generation method. Consequently, only the representative results from the five test repetitions are presented in the subsequent sections.

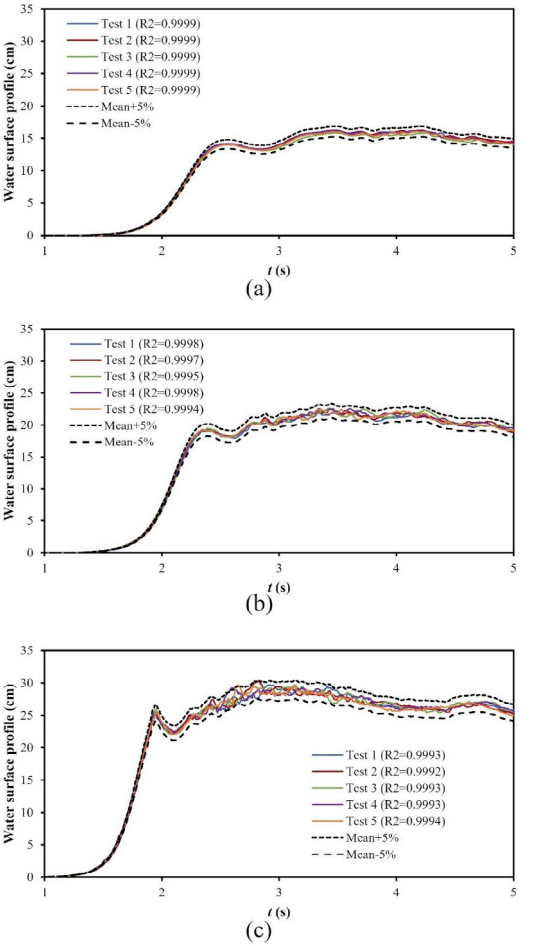

Figure 3. Repeatability for wave profile propagation measured at H1 for (a) 40 mm, (b) 70 mm and (c) 100 mm wave conditions.

Bores and Surges

Basically, the generation of tsunami-like waves manifests as both bores and surges. Bores are formed following the breaking of the solitary wave and propagate on the wet bed, while surges represent incoming waves that move along the dry bed. Figure 4 shows visual observations of both bores and surges developed in the experiments. Figure 4(a) illustrates a wet bed bore characterized by a turbulent wave with pronounced air entrainment and high aeration in the front region. This accumulation of high turbulence, as noted by Yeh (1991) and Heller et al. (2005), releases a substantial amount of energy upon reaching the dry shore, resulting in significant inland inundation and extensive damage to inland located structures. In contrast, Figure 4(b) displays a dry bed surge, which exhibits a relatively gentle sloping wave with a non-aerated front. Both wet bed bore and dry bed surge achieve maximum flow depth after some distance from the tip (Figure 4(c)). These findings align with the insights of Ramsden (1996), Nouri et al. (2010) and Wüthrich et al. (2018), regarding the differences between bores and surges.

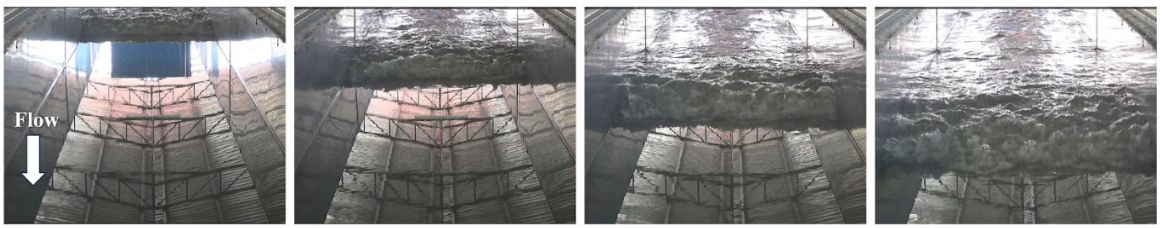

(a) Wet bed bores advancing across offshore region

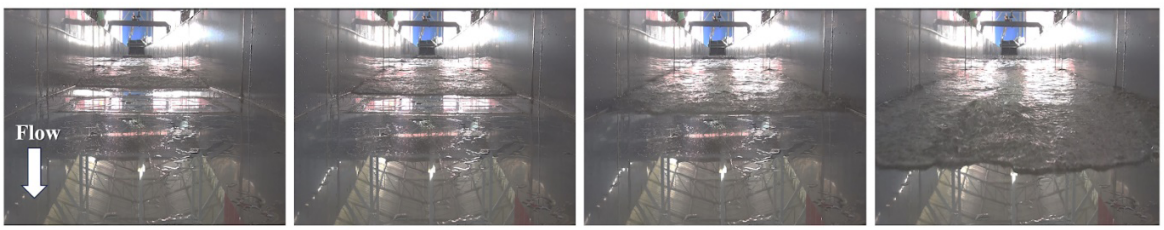

(b) Dry bed surges moving towards onshore region

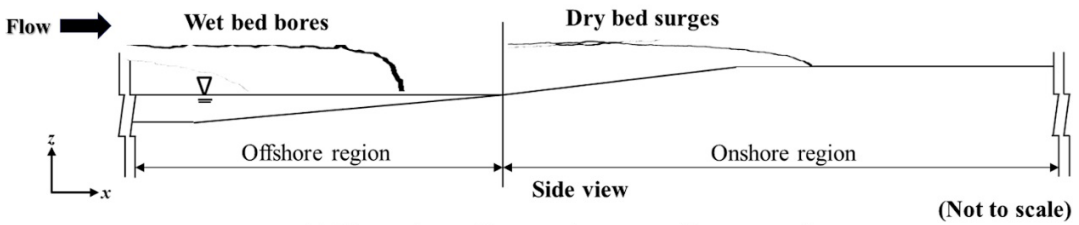

(c) Illustrations of bore and surge profile propagation

Figure 4. Propagation of tsunami-like waves across the wave flume (h_{max} = 70 mm).

Flow Depths

The spatial-temporal evolution of flow depth nearshore, for all wave conditions, are presented in Figure 5. It is noteworthy in Figure 5 that the initial abrupt increase in water depth observed at each wave gauge marks the passage of the wave front. At the shoreline (H2), the advancing wave displays bore-like characteristics, with a rapid increase in water depth at the wave front. In contrast, at H3, the front of the wave surge exhibits a shallower flow depth, rising gradually and reaching a quasi-steady state, characterized by the fully developed maximum depth. In the later stages, the water level begins to decrease, a result of the diminishing reservoir volume upstream of the flume. Notably, as the wave progresses up

the 1:125 sloping bed (transition of H2 and H3), the observed reduction in maximum flow depth can be attributed to the viscous and diffusive behavior of the flow, as elucidated by Wüthrich et al. (2018).

This study primarily focused on the dry bed surge at the onshore location, situated 3.225 m horizontally and 20 mm vertically from the shoreline. By using the average surge speed calculated from Figure 5, the tip region of the flow depth at H3 is transformed from the time domain to the distance domain for each wave condition. This approach has been previously employed by Shafiei et al. (2016), and Figure 6 depicts the resulting surge front profile from this transformation. The transformed surge front profile can be likened to a photograph of the leading front of the surge captured from the side of the flume. The results indicate that higher waves exhibit steeper sloping fronts of surges, with observed angles of approximately 2.13°, 2.80°, and 3.15° to the horizontal for 40, 70, and 100 mm wave conditions, respectively (Table 1).

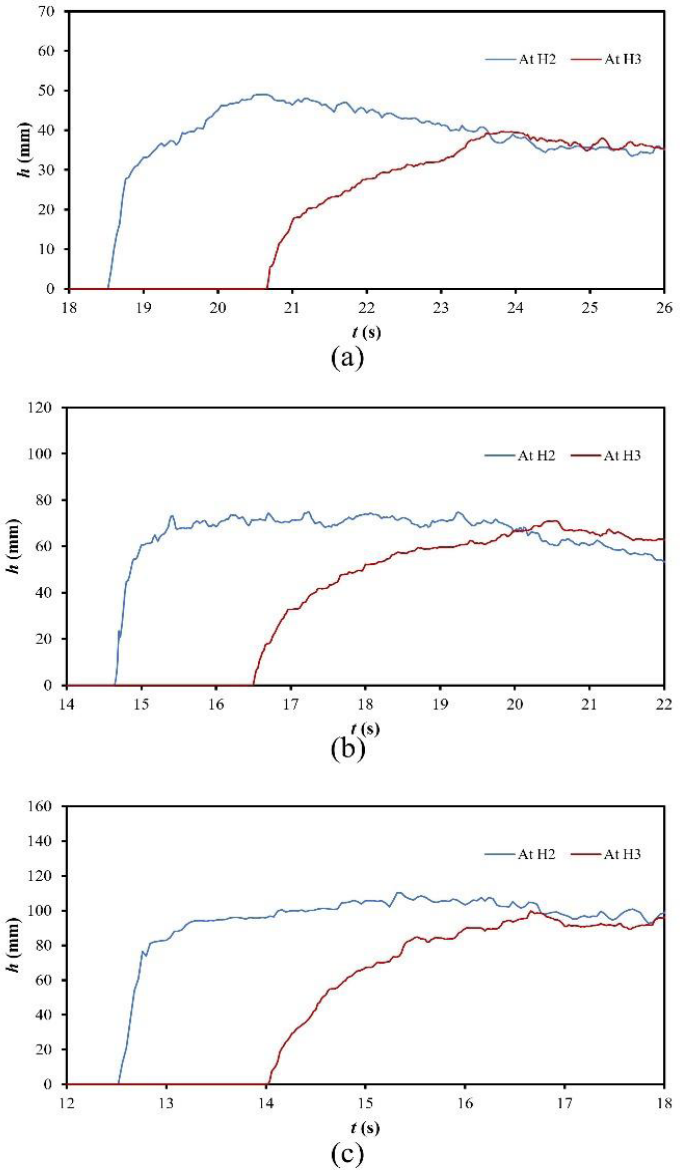

Figure 5. Evolution of flow depth at nearshore for (a) 40 mm, (b) 70 mm, and (c) 100 mm wave conditions.

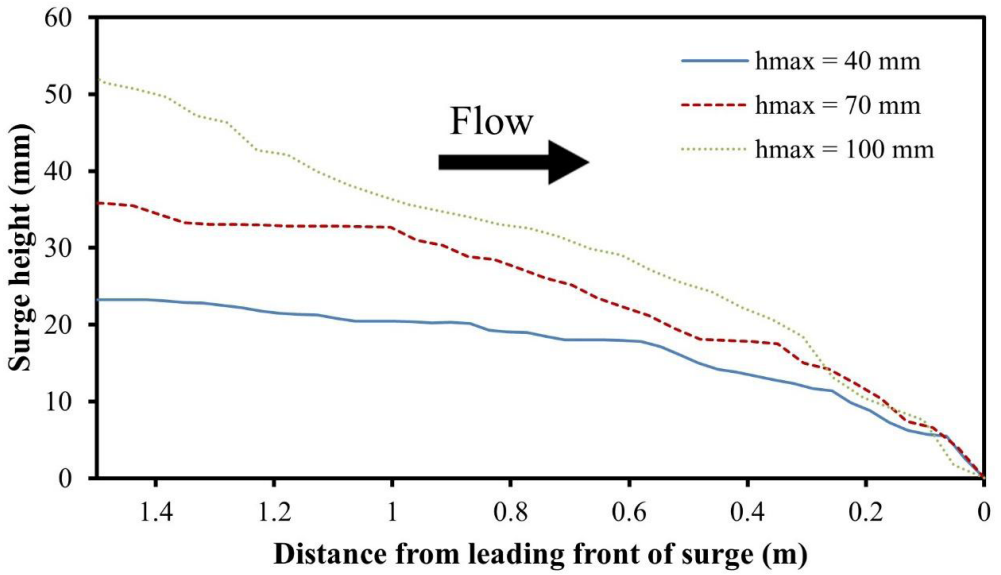

Figure 6. Computed surge front profile in relation to its leading front. Note: 0 on the *x*-axis indicates the leading front.

Flow Velocities

Figure 7 displays the representative time histories of flow velocities at V2 and V3, for all wave conditions. It is noticeable that the maximum flow velocity is reached at the wave front. Notably, there is a significant disparity in the flow velocity of the dry bed surge at V3, which exhibits a higher peak velocity compared to the wave arrival at V2. From the figures, this peak velocity discrepancy is more pronounced for the higher wave condition, which can be attributed to the release of energy from the high turbulence of a broken wave on the dry shore, as previously mentioned. Subsequently, there is a gradual deceleration until the flow becomes relatively uniform during the quasi-steady phase (Figure 7).

The non-dimensionalized flow velocities of dry bed surges for all three wave conditions are presented in Figure 8, in which the time has been shifted so that T = 0 s denotes the surge arrival time at V3. Figure 8 shows that measurements for lower wave conditions exhibit a more fluctuating behavior, particularly during the quasi-steady flow phase. This behavior results of water surface fluctuations in shallow water flows. The experimental data regarding deceleration behind the surge front is also compared with the expression of Wüthrich et al. (2018) in

$$\frac{u}{U} = 1 - c \cdot \tanh\left(b \cdot T \sqrt{\frac{g}{d_o}} \right) \quad (1)$$

which b and c are the empirical parameters, u and U denote the flow velocity and wave front celerity, respectively. In this work, the initial impoundment depth, d_o is replaced by h_{max}. The good correspondence seen in Figure 8 suggests that the flow velocities behind the surge front can be predicted using Eq. (1), with an ad hoc value of b = 0.04 used in this study.

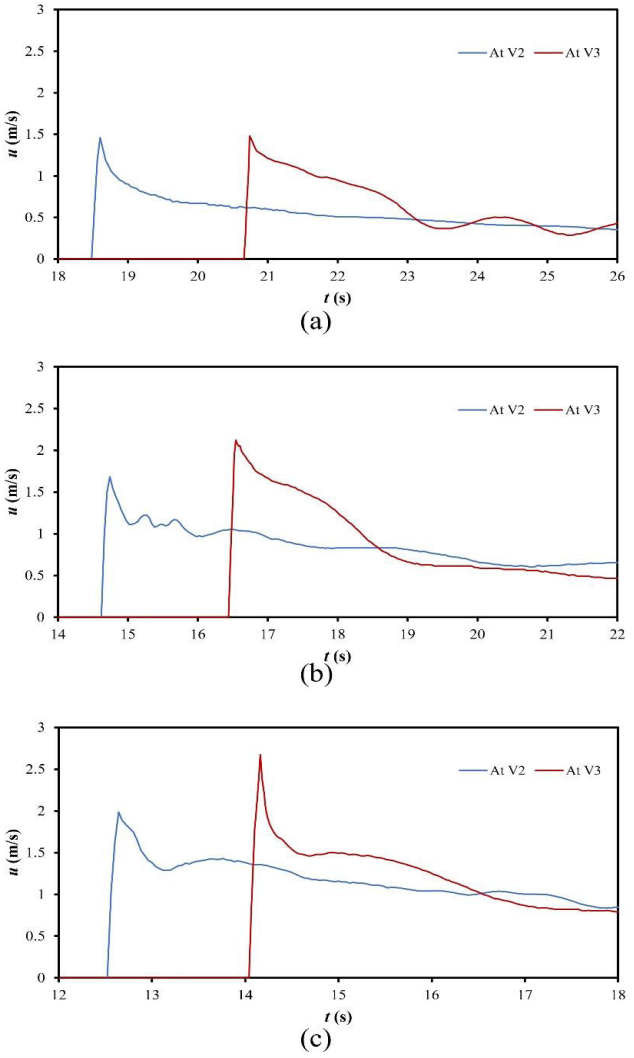

Figure 7. Time histories of nearshore flow velocities for (a) 40 mm, (b) 70 mm, and (c) 100 mm wave conditions.

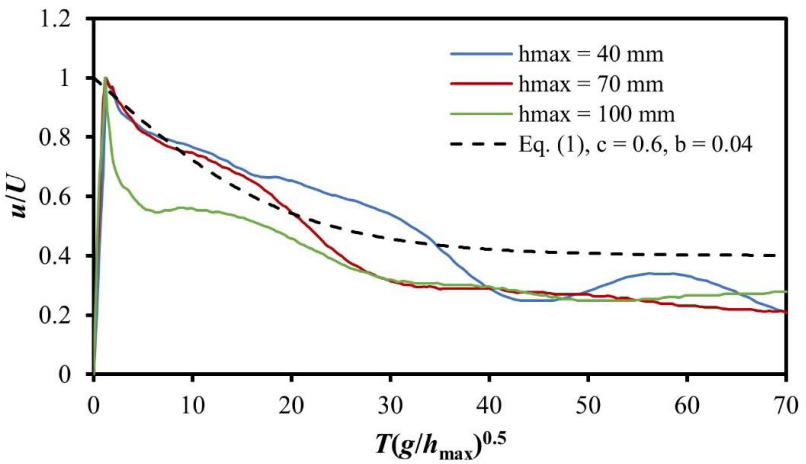

Figure 8. Dimensionless flow velocities for dry bed surges at V3.

Flow Depth-Velocity Relationship

In this section, we explore the correlation between the flow depth and velocity of the dry bed surge at the onshore location. The Froude number (*Fr*) for a dry bed surge is shown in Figure 9. Notably, *Fr* shown herein is defined as $u\ (gh)^{-0.5}$. For all three wave conditions, the *Fr* values exhibit a similar trend over time. The highest *Fr* value, approximately 6, is observed at the surge front.

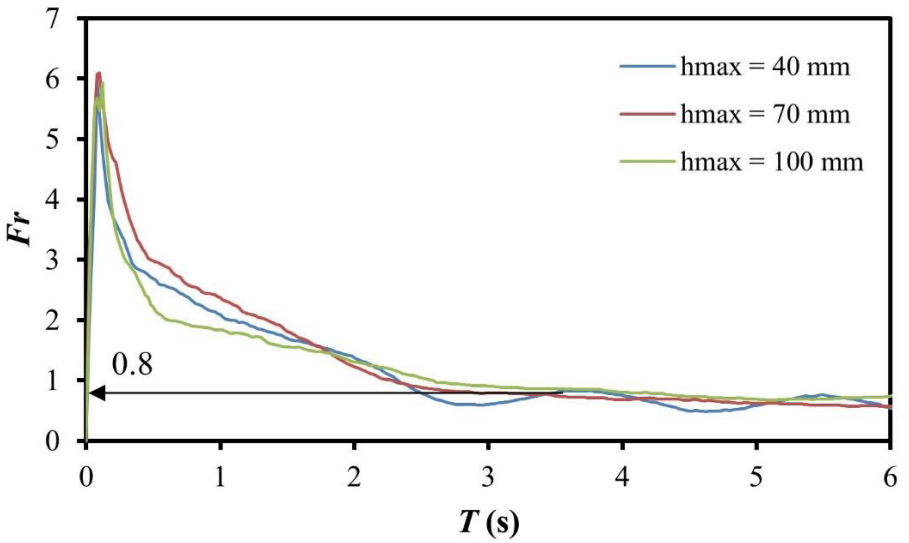

Figure 9. Computed Froude number (*Fr*) for different wave conditions.

This value subsequently decreases to around 2 at approximately T = 1 s, and further drops to less than 1 once the wave reaches the quasi-steady state. Notably, Asakura et al. (2002) evaluated the Froude number of a tsunami wave when the inundation depth is at its maximum. In this study, the maximum flow depth is achieved during the quasi-steady flow phase (T > 3 s). Consequently, the computed *Fr* values are approximately 0.8 (Figure 9).

Determining flow quantities (flow depth and velocity) becomes a challenging task, particularly when laboratory tests are not available. Therefore, expressing the maximum flow velocity as a function of the maximum flow depth is essential, as follows,

$$U = \alpha\sqrt{gh_{\max}} \qquad (2)$$

in which α is a constant. In light of some relevant literature, the results obtained from this study are compared with various formulas proposed by Murty (1977), Kirkoz (1983), Iizuka and Matsutomi (2000), Bryant (2001), Matsutomi and Okamoto (2010), FEMA (2012), Shafiei et al. (2016), and Wüthrich et al. (2018), as tabulated in Table 2. The results are found to align well with the maximum flow velocities when an α value of 2.6 is used (Figure 10). This finding reveals a significant disparity among the formulas proposed by different researchers. One plausible explanation for such disparities could be attributed to the characteristics of the dam break flow generated in this study. In dam break scenarios, flow parameters like depth and velocity are closely related to the impoundment reservoir volume, which is the amount of water stored behind the dam gate. Differences in both the reservoirs base and impoundment depth potentially contribute to the observed disparities.

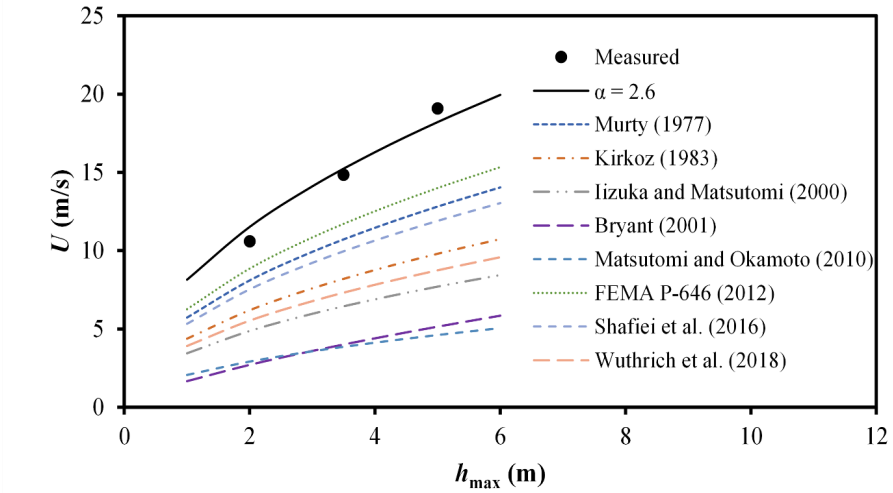

Figure 10. Correlation between flow celerity and maximum flow depth at prototype scale.

Table 2. Coefficient α in Eq. (2).

Reference	α value	Remarks
Murty (1977)	1.83	Based on observational data
Kirkoz (1983)	1.4	-
Iizuka and Matsutomi (2000)	1.1	Based on experimental data and field tsunami survey data
Bryant (2001)	$U = 1.67(h_{max}^{0.7})$	Based on observational data
Matsutomi and Okamoto (2010)	0.66	Based on field data and theoretical data
FEMA (2012)	2	Based on Dames and Moore (1980) of prior laboratory research on tsunami loading
Shafiei et al. (2016)	1.7	Based on experimental data
Wüthrich et al. (2018)	1.25	Based on experimental data

However, it is noteworthy that this study results align with the observed wave characteristics during the 2004 tsunami event near Penang Island. Documentaries from DID (2005), Yalciner et al. (2005), Komoo and Othman (2006), Horton et al. (2008), Koh et al. (2009), and video clips obtained from eyewitnesses in tsunami-affected regions in Penang Island were analyzed, and a summary is presented in Figure 11. The Froude number values, computed based on the flow celerity and the observed maximum runup height, vary from 1.05 to 2.59 in Penang Island during the 2004 IOT. This range means that the upper limit of the actual event is accurately reflected in this study results.

Incident place	Estimated travelled distance (m)	Estimated travelled time (s)	Computed flow velocity (m/s)	Observed maximum run-up height (m)	*Fr*
Tanjung Bungah	264.09	19.44	13.59	2.20 – 2.80	2.39 - 2.59
	40.00	3.60	11.11		
Gurney Drive	32.65	5.48	5.95	3.25	1.05

Figure 11. Froude number computed for tsunami wave approaching Penang Island, Malaysia.
Source: DID (2005); Yalciner et al. (2005); Horton et al. (2008); Koh et al. (2009)

In calculating the maximum hydrodynamic force on a structure, Yeh (2007) emphasized the importance of considering the maximum momentum flux (hu2)max at the location where the structure is absent. Recognizing the significant influence of flow depth and velocity on wave-induced forces, this study thus computed the momentum flux for all three wave conditions, as depicted in Figure 12. The momentum flux displays a consistent pattern over time with the flow velocity time histories (as in Figure 8). For lower wave conditions (h_{max} = 40 and 70 mm), the momentum flux peaks in the initial stage (T < 1 s), corresponding to the period of high flow velocity. In contrast, a subsequent increase in momentum flux after 1 s is observed in the case of the 100 mm wave condition. This is attributed to the rapid flow increase and a high-velocity head at that moment. Following this, the momentum flux gradually decreases at T > 2 s and enters a sustained phase.

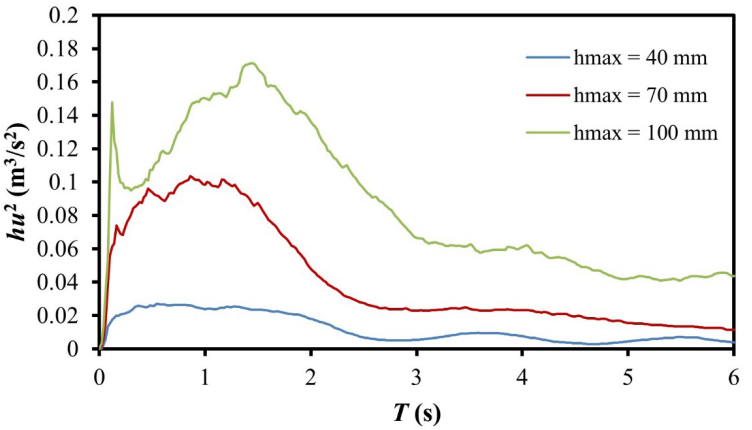

Figure 12. Computed momentum flux (hu^2) for different wave conditions.

In the study conducted by Wüthrich et al. (2018), a ratio denoted as $h[(hu^2)_{max}](h_{max})^{-1}$ was introduced and investigated. This ratio represents the relation between the water level at the occurrence of maximum momentum flux and the maximum flow depth. A ratio of 1 suggests that the maximum momentum flux coincides with the water level equal to the maximum flow depth. Figure 13 presents the ensemble-averaged surge heights from this study. The results align with previous findings reported by Yeh (2007) and Wüthrich et al. (2018) showing that the maximum momentum flux precedes the attainment of the maximum flow depth for all three wave conditions (ratio < 1). The experimental data also exhibits a reasonable agreement with the approach proposed by Chock (2015), represented by the dashed line in Figure 13. However, it appears that the Chock (2015) approach may underestimate the surge height by approximately 25% for the 100 mm wave condition, suggesting its potential inapplicability for cases with higher flow depths.

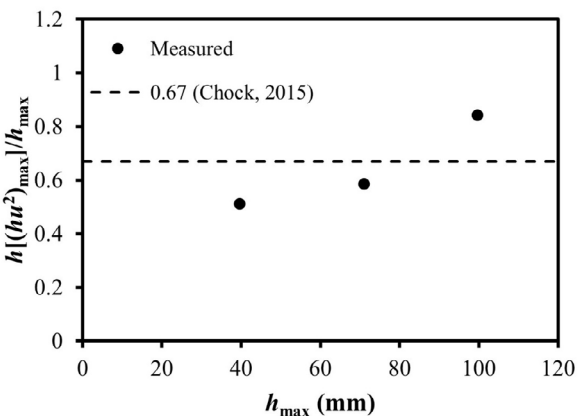

Figure 13. Ensemble-averaged surge height (for each wave condition) at occurrence of maximum momentum flux [$(hu^2)_{max}$].

CONCLUSIONS

The experiments, conducted at a scale of 1:50, successfully replicated tsunami-like waves, revealing the presence of both bores and surges, with maximum flow depths ranging from 2.5 m to

5 m and front celerity spanning from 10.6 m s^{-1} to 19.9 m s^{-1} in prototype scale. The findings offer valuable insights for improving resilience and preparedness in the context of potential inundation scenarios. In summary, the study indicates the following key points:

- Wet bed bores are characterized by rapid increases in water depth and significant air entrainment in the front region. In contrast, dry bed surges manifest as gentler sloping waves with no aeration in the front. The maximum flow depth decreases as waves progress from the shoreline to the dry shore region on a 1:125 sloping bed.
- Flow velocities reach their maximum at the wave front. Dry bed surges exhibit higher peak velocities compared to wet bed bores due to energy release from broken waves on the dry shore. The deceleration behind the surge front can be predicted using Eq. (1), with an ad hoc value of b = 0.04, c = 0.6.
- Momentum flux follows similar trends to flow velocity time histories. For the highest wave condition, a subsequent increase in momentum flux occurs after 1 s, attributable to the rapid flow and a high-velocity head.
- The maximum momentum flux precedes the maximum flow depth based on the ratio $h[(hu^2)_{max}](h_{max})^{-1}$, with a reasonable agreement with the Chock (2015)'s approach, except for the 100 mm wave condition, which may be underestimated by approximately 25%.

ACKNOWLEDGEMENT

The experimental setup was funded by MOSTI under ScienceFund Research Grant (04-01-05-SF0562) and JICA Project for AUN/SEED-Net via Collaborative Research for Alumni (CRA) 2013 (USM CRA-1301). The authors also express their gratitude to the reviewers for their valuable contributions and insightful suggestions.

AUTHOR CONTRIBUTIONS

W.C.M.: Conceptualization; Investigation; Methodology; Writing – original draft.

T.L.L.: Supervision; Funding Acquisition; Writing – review & editing.

H.T.P.: Supervision; Writing – review & editing.

REFERENCES

Abdullah, K., Tan, K. & Ghazali, N. 2005. No more in the comfort zone–Malaysia's response to the December 2004 Tsunami. *In*: *International Hydrography and Oceanography Conference and Exhibition* (pp. 1-28).

Adam, M. R. B. 2011. Numerical simulation as guidance in making tsunami hazard map for Labuan Island. *Bulletin of the International Institute of Seismology and Earthquake Engineering,* 45**,** 121–126.

Ahmadun, F. l.-R., Wong, M. M. R. & Said, A. M. 2020. Consequences of the 2004 Indian ocean tsunami in Malaysia. *Safety science,* 121**,** 619–631.

Asakura, R., Iwase, K., Ikeya, T., Takao, M., Kaneto, T., Fujii, N. & Ohmori, M. 2002. The tsunami wave force acting on land structures. *Coastal Engineering 2002: Solving Coastal Conundrums*, 1191–1202.

Basri, S. N., Fujii, Y., Shibazaki, B. & Yanagisawa, H. 2013. Study on tsunami inundation simulation in the northwestern coast of Sabah, Malaysia. *Bulletin of the International Institute of Seismology and Earthquake Engineering,* 47, 133–138.

Bryant, E. 2001. *Tsunami: The Underrated Hazard*. Cambridge, Cambridge University Press.

Chanson, H. 2006. Tsunami surges on dry coastal plains: Application of dam break wave equations. *Coastal Engineering Journal,* 48**,** 355–370.

Chock, G. 2015. The ASCE 7 tsunami loads and effects design standard for the United States. In: Esteban, M., Takagi, H. & Shibayama, T. *Handbook of coastal disaster mitigation for engineers and planners.* (pp. 437-460). Amsterdam: Elsevier.

Cross, R. H. 1967. Tsunami surge forces. *Journal of the waterways and harbors division,* 93**,** 201–231.

Dao, M. H., Tkalich, P., Chan, E. S. & Megawati, K. 2009. Tsunami propagation scenarios in the South China Sea. *Journal of Asian Earth Sciences,* 36**,** 67–73.

DID (Department of irrigation and Drainage). 2005. Laporan penyiasatan pasca-tsunami 26 Disember 2004. Kuala Lumpur. Malaysia, Department of Irrigation and Drainage.

FEMA (Federal Emergency management Agency). 2012. *Guidelines for design of structures for vertical evacuation from tsunamis*. 2. ed. Washington, D.C, Federal Emergency Management Agency.

Heger, M. P. & Neumayer, E. 2019. The impact of the Indian Ocean tsunami on Aceh's long-term economic growth. *Journal of Development Economics,* 141**,** 102365.

Heller, V., Unger, J. & Hager, W. 2005. Tsunami run-up-a hydraulic perspective. *Journal of Hydraulic Engineering,* 131, 743–747.

Horton, B., Bird, M., Birkland, T., Cowie, S., Eong, O. J., Hawkes, A., Khoon, G. W., Law, L., Macgregor, C., Shau-Hwai, A. T., Sa, T. T. & Yasin, Z. 2008. Environmental and socioeconomic dynamics of the Indian Ocean tsunami in Penang, Malaysia. *Singapore Journal of Tropical Geography,* 29, 307–324.

Iizuka, H. & Matsutomi, H. 2000. Damage due to flood flow of tsunami. *Coastal Engineering Proceedings*, 381–385.

Ismail, H. & Wahab, A. K. A. 2011. *Numerical experiments on tsunami propagation into the Straits of Malacca. In:* KOH, H., PHILIP, L.-F. L. & TEH, S. Y. (Ed.) *Tsunami Simulation for Impact Assessment* (pp. 174-185). Pulau Pinang: Universiti Sains Malaysia Press.

Karim, F., Ismail, M. & Izani, A. 2010. Estimation of expected maximum water level due to tide and tsunami interaction along the coastal belts of Penang Island in Peninsular Malaysia. *Science of Tsunami Hazards,* 29, 127–138.

Kirkoz, M. S. 1983. Breaking and run-up of long waves, tsunamis: their science and engineering. *In*: *Proceedings of the 10th IUGG International Tsunami Symposium*.

Klettner, C., Balasubramanian, S., Hunt, J., Fernando, H., Voropayev, S. & Eames, I. 2012. Draw-down and run-up of tsunami waves on sloping beaches. *Proceedings of the Institution of Civil Engineers - Engineering and Computational Mechanics,* 165, 119–129.

Koh, H. L., Teh, S. Y., Liu, P. L. F., Ismail, A. I. M. & Lee, H. L. 2009. Simulation of Andaman 2004 tsunami for assessing impact on Malaysia. *Journal of Asian Earth Sciences,* 36, 74–83.

Komoo, I. & Othman, M. 2006. *The 26.12.04 tsunami disaster in Malaysia*: An environmental, socio-economic and community well-being impact study. Kuala Lumpur, Akademi Sains Malaysia.

Liu, P. L. F., Wang, X. & Salisbury, A. J. 2009. Tsunami hazard and early warning system in South China Sea. *Journal of Asian Earth Sciences,* 36, 2-12.

Matsutomi, H. & Okamoto, K. 2010. Inundation flow velocity of tsunami on land. *Island Arc,* 19, 443–457.

Mazni, A. 2012. Tsunami numerical simulation around Sulu Sea and Celebes Sea. *Bulletin of the International Institute of Seismology and Earthquake Engineering,* 46, 109–114.

Mokhtar, Z. A. B., Imamura, F. & Koshimura, S. 2008. Study on appropriate modeling of tsunamis in Malaysia for risk evaluation. *Bulletin of the International Institute of Seismology and Earthquake Engineering,* 42, 139–144.

Moon, W. C., Lau, T. L., Puay, H. T. & Lum, P. T. 2020. *Experimental modelling of tsunami-like waves approaching the gentle coast of Malaysia*. *In*: *Articles Compilation: Thesis in 5 Minutes* (pp. 14-20). Negeri Sembilan: MNNF Publisher.

Moon, W. C., Sidek, L. M., Lau, T. L., Puay, H. T., Majid, T. A., Wahab, A. K. A. & Teo, F. Y. 2022. A Shared Vision on the 2004 Indian Ocean Tsunami in Malaysia: Hazard Assessments, Post-Disaster Measures and Research. *Journal of Marine Science and Engineering,* 10, 1088.

MOSTI (Ministry of Science Technology & Innovation). 2009. *Seismic and tsunami hazards and risks study in Malaysia*. *Summary for policy makers.* Kuala Lumpur: Academy of Sciences Malaysia.

Murty, T. S. 1977. *Seismic sea waves: Tsunamis*. Fisheries and Marine Service. Ottawa, Department of Fisheries and the Environment.

Nelson, S. 2011. *The course note on tsunami* [Online]. Available from: https://earthsci.org/education/teacher/basicgeol/tsumami/tsunami.html Access date: 2019 Jan. 2.

Nouri, Y., Nistor, I., Palermo, D. & Cornett, A. 2010. Experimental investigation of tsunami impact on free standing structures. *Coastal Engineering Journal,* 52, 43–70.

Nurashid, N. I., Shibazaki, B., Fujii, Y. & Yanagisawa, H. 2013. Tsunami inundation modeling along the east coast of Sabah, Malaysia for potential earthquakes in Sulu Sea. *Bulletin of the International Institute of Seismology and Earthquake Engineering,* 47, 127–132.

Oktari, R. S., Nugroho, A., Fahmi, M., Suppasri, A., Munadi, K. & Amra, R. 2021. Fifteen years of the 2004 Indian Ocean Tsunami in Aceh-Indonesia: Mitigation, preparedness and challenges for a long-term disaster recovery process. *International Journal of Disaster Risk Reduction,* 54, 102052.

Pedersen, C., Latif, Z. A. & Lai, C. 2010. Tsunami modelling and risk mapping for east coast of Sabah, Malaysia. *Coastal Engineering Proceedings*, 1(32), 55–64.

Ramsden, J. D. 1996. Forces on a vertical wall due to long waves, bores, and dry-bed surges. *Journal of Waterway, Port, Coastal, and Ocean Engineering,* 122, 134–141.

Shafiei, S., Melville, B. W. & Shamseldin, A. Y. 2016. Experimental investigation of tsunami bore impact force and pressure on a square prism. *Coastal Engineering,* 110, 1–16.

Shaluf, I. M. & Ahmadun, F. l.-R. 2006. Disaster types in Malaysia: an overview. *Disaster Prevention and Management: An International Journal,* 15, 286–298.

Teh, S., Koh, H., Moh, Y., DeAngelis, D. & Jiang, J. 2011. Tsunami risk mapping simulation for Malaysia. *WIT Transactions on the Built Environment,* 119, 3–14.

Wüthrich, D., Pfister, M., Nistor, I. & Schleiss, A. J. 2018. Experimental study of tsunami-like waves generated with a vertical release technique on dry and wet beds. *Journal of Waterway, Port, Coastal, and Ocean Engineering,* 144, 04018006.

Yalciner, A., Ghazali, N. & Abd Wahab, A. 2005. *Report on December 26, 2004, Indian Ocean Tsunami, field survey on July 09-10, 2005 north west of Malaysia, Penang and Langkawi Islands*. Townsville, Australian Institute of Marine Science.

Yeh, H. 2007. Design tsunami forces for onshore structures. *Journal of Disaster Research,* 2, 531–536.

Yeh, H. H. 1991. Tsunami bore runup. *Natural Hazards,* 4, 209–220.

Yeh, H. H. & Ghazali, A. 1988. On bore collapse. *Journal of Geophysical Research: Oceans,* 93, 6930–6936.

Yeh, H. H. & Mok, K. M. 1990. On turbulence in bores. *Physics of Fluids A: Fluid Dynamics,* 2, 821–828.